A Unified Approach to Photon and Beta Particle Dosimetry

Peter K. Leichner

Department of Radiology, University of Nebraska Medical Center, Omaha, Nebraska

The purpose of this investigation was to develop a unified and practical method for photon and beta particle dosimetry. **Methods:** This was achieved by developing a point-source function that is equally valid for photons and beta particles. This function contains four fitting parameters. These were computed on the basis of Berger's tables for a wide range of photon and beta particle energies. Explicit formulas were derived for the absorbed fraction within and outside of spheres containing a uniform distribution of activity. For photons, calculations of the absorbed fraction at the center of spheres were compared with the results of Monte Carlo calculations. The two methods yielded essentially identical results, validating the approach used in this study. **Results:** The results of this study show that there are absorbed-dose gradients as a function of distance from the center of a sphere. These should be taken into account in absorbed-dose calculations. For beta particles, it is shown explicitly that for spheres with a radius of 0.08 cm, absorbed-dose rates from ^{131}I and ^{90}Y beta particles are equal. **Conclusion:** An important feature of this work is that calculations can be made on the macroscopic, cellular and subcellular levels. The approach employed and results obtained in this work should be particularly useful for tumor dosimetry in radionuclide therapy and applicable radiobiological investigations.

Key Words: dosimetry; photon dosimetry; beta particle dosimetry

J Nucl Med 1994; 35:1721–1729

I t has long been recognized that knowledge of absorbed-dose distributions arising from distributed sources of radioactivity is of fundamental importance in physics, biology and nuclear medicine (1–3). In particular, the use of beta particle point-source functions or point kernels, in conjunction with the superposition principle (4), has led to a better understanding of absorbed-dose distributions for a variety of source and absorber configurations (1–12). Point-source functions have also been employed in photon dosimetry; some authors have suggested that these functions be the same or nearly the same as for beta particles (1,3,5) and

others have used completely different functions for beta particle and photon dosimetry (7,12).

In the present article it is shown that a previously introduced point-source function for beta particles (11) is equally valid for photons. This function is empirical and four fitting parameters embedded in it were calculated on the basis of Berger's tables for the energy deposition in water by photons from point isotropic sources (13) and the absorbed dose distribution around point sources of beta particles (14).

The fact that one function can be used to calculate absorbed-dose distributions for photons and beta particles provides considerable computational advantages in analytical and numerical solutions of dosimetry problems. This is demonstrated by deriving an analytical solution of the absorbed-dose distributions within and outside of spheres containing a uniform distribution of photon or beta particle activity. The analytical solution should prove useful in the computation of S factors for tumors which can be modeled as spheres, which has been done in radioimmunotherapy (RIT) dosimetry (15–17). It is emphasized, however, that the equations provided in the Appendix obviate the need for tables of S factors for spherical volume sources of photons and beta particles. Indeed, they provide information about absorbed-dose gradients that are not included in tables and would be difficult, if not impossible, to tabulate. More generally, these solutions are applicable to the dosimetry of a variety of radionuclides, including those that are of radiobiological interest.

The notation for absorbed-dose rate and dose developed by the MIRD Committee (18) is used throughout this article. The MIRD schema provides a flexible and compact set of equations in terms of absorbed fractions which is particularly useful in macrodosimetry and dosimetry on the cellular and subcellular levels. The complexity of formulas for computing absorbed fractions depends on the point-source function used and the geometry under consideration. For spherical geometry and the point-source function employed in this article, these formulas are quite lengthy and have, therefore, been put into an appendix. The results presented in the body of this article are focused on several aspects of absorbed-dose calculations. These include an examination of gradients in absorbed-dose rates

within and outside of spherical source volumes of photons and beta particles.

METHODS

Photons

In conformity with the MIRD convention (18), Berger (13) expressed the absorbed-dose rate at a distance r from a point source of monoenergetic photons in an unbounded homogeneous medium in the form

$$\dot{D}(r) = A\Delta\Phi(r), \qquad \text{Eq. 1}$$

with

$$\Delta = nE. \qquad \text{Eq. 2}$$

The quantity A is the source activity, Δ is the energy emitted per unit cumulated activity defined in Equation 2; $\Phi(r)$ is the point isotropic specific absorbed fraction, n is the number of photons per nuclear transformation and E is the photon energy. For photons

$$\Phi(r) = \left[\frac{\mu_{en}}{\rho}\frac{1}{4\pi r^2}e^{-\mu r}\right]B_{en}(\mu r), \qquad \text{Eq. 3}$$

where μ_{en} is the linear photon energy-absorption coefficient at the source energy, ρ is the mass density, and μ is the linear photon attenuation coefficient. The factors in square brackets in Equation 3 represent the contribution of primary photons to the absorbed dose rate. Units associated with the various quantities in Equations 1–3 are provided by Berger (13) and the MIRD Committee (18). The quantity $B_{en}(\mu r)$ is the energy absorption buildup factor, a dimensionless function which takes into account the contribution of scattered photons to the absorbed dose rate.

Berger (13) used a moment method for numerical calculations of the buildup factor for photon energies ranging from 15 keV to 3 MeV and distances from the source ranging from 0.05 to 20 mean free paths. At each photon energy, the buildup factor was also expressed in terms of a ten-term polynomial. As discussed by Berger (13), it would be more convenient to approximate the buildup factor by other formulas involving fewer numerical parameters. This has been achieved in the present work. It was shown subsequently (19) that Berger's results (13) were consistent with Monte Carlo calculations of the photon transport in large soft-tissue volumes.

In the present work, tabulated values of the buildup factors were analytically represented by the function

$$B_{en}(\mu r) = 1 + [c_1(\mu r) + c_2(\mu r)^2 + c_3(\mu r)^3]e^{-c_4\mu r}, \qquad \text{Eq. 4}$$

and the fitting coefficients c_1 to c_4 were computed from the tabulated values of B_{en} using a nonlinear least-squares fitting procedure ($20,21$). For $\mu r = 0$, this function satisfies the requirement of being equal to unity. It also satisfies the requirement of increasing linearly with μr for small values of μr (13). The expression for B_{en} in Equation 4 is similar to that used for calculating absorbed fractions for small volumes containing photon-emitting radioactivity (22). A principal difference between the expression for B_{en} in the present work and that which was previously used is the coefficient c_4 in the exponent of Equation 4. The presence of this coefficient removes the small-volume constraint and, as shown in the results section, absorbed-dose calculations based on Equation 4 can be made for any finite volume.

For a monoenergetic photon source volume, the absorbed-dose rate may be written in the form

$$\dot{D}(r) = CA\phi(r), \qquad \text{Eq. 5}$$

where C is the mean activity per unit mass (Bq/kg or μCi/g) and ϕ is the absorbed fraction. In contrast to the specific absorbed fraction, the absorbed fraction is dimensionless and ranges in numerical value from 0 to 1. The relation between the absorbed fraction and the specific absorbed fraction is given by (22)

$$\phi = \rho \int \Phi(r)\, dV. \qquad \text{Eq. 6}$$

From Equations 3–6 it follows that the absorbed fraction for photons may be written in the form

$$\phi = \mu_{en} \int \frac{e^{-\mu r}}{4\pi r^2} \{1 + [c_1(\mu r) + c_2(\mu r)^2 + c_3(\mu r)^3]e^{-c_4\mu r}\}\, dV. \qquad \text{Eq. 7}$$

The evaluation of this integral for spherical geometry is outlined in the appendix and explicit formulas are presented for the absorbed fraction as a function of distance from the center within and outside of spheres containing uniform distributions of activity.

Beta Particles

According to the MIRD schema ($13,18$), the absorbed-dose rate for beta particles may be written in the form

$$\dot{D}_\beta(r) = A\Delta\Phi_\beta(r), \qquad \text{Eq. 8}$$

where A is the source activity and $\Delta = n_\beta E_{av}$ (n_β is the number of beta particles per nuclear transformation and E_{av} is the weighted average beta particle energy). The quantity $\Phi_\beta(r)$ is the point isotropic specific absorbed fraction for beta particles. The absorbed-dose distributions for beta particles in Berger's tables (14) were compiled in terms of a scaled absorbed-dose distribution function, $F_\beta(\xi)$, that is a function of the ratio $\xi = r/r_{90}$. The relation between $F_\beta(\xi)$ and $\Phi_\beta(r)$ is given by

$$F_\beta(\xi)/r_{90} = 4\pi\rho r^2\Phi_\beta(r). \qquad \text{Eq. 9}$$

From Equations 8 and 9 and the results in Leichner et al. (11), it follows that the beta particle dose rate may also be written as

$$\dot{D}_\beta(r) = A\Delta\frac{F_\beta(\xi)/r_{90}}{4\pi\rho r^2} = A\Delta\frac{G(r)}{4\pi\rho r^2}. \qquad \text{Eq. 10}$$

In (11) it was shown that the ratio $F_\beta(\xi)/r_{90}$ for beta particles was accurately represented by the function

$$G(r) = G_0\{e^{-\mu'r} + [d_1(\mu'r) + d_2(\mu'r)^2 + d_3(\mu'r)^3]e^{-d_4\mu'r}\}, \qquad \text{Eq. 11}$$

where d_1 to d_4 are fitting coefficients which were obtained from a least-squares fit, and μ' is the apparent absorption coefficient for beta particles (3). In Equation 11, the quantity G_0 is defined by

$$G_0 = G(r = 0) = F_\beta(0)/r_{90}. \qquad \text{Eq. 12}$$

For a volume source of beta particles, the absorbed dose rate may be written in the form

$$\dot{D}_\beta(r) = CA\phi_\beta(r), \qquad \text{Eq. 13}$$

where $\phi_\beta(r)$ is the absorbed fraction for beta particles. From Equations 6, 10 and 11 it follows that the absorbed fraction may be calculated from

TABLE 1
Numerical Values of the Fitting Coefficients c_1, c_2, c_3 and c_4 for Photons

Energy (MeV)	c_1	c_2	c_3	c_4
0.015	0.247	−0.0298	0.00321	0.146
0.02	0.552	−0.0515	0.00631	0.135
0.03	1.32	0.00100	0.00297	0.0496
0.04	2.48	0.114	0.00142	0.000685
0.05	2.83	0.632	0.00662	0.000688
0.06	2.68	1.12	0.0365	0.000701
0.08	2.40	1.21	0.152	0.000728
0.10	2.28	0.979	0.215	0.000732
0.15	1.72	0.763	0.184	0.000782
0.20	1.58	0.602	0.128	0.00200
0.30	1.22	0.564	0.0539	0.00120
0.40	1.16	0.502	0.0208	0.00559
0.50	1.07	0.409	0.00964	0.00561
0.60	1.10	0.328	0.0131	0.0201
0.80	1.05	0.254	0.0140	0.0429
1.00	0.960	0.193	0.0152	0.0560
1.50	0.921	0.122	0.00775	0.0613
2.00	0.809	0.0786	0.00749	0.0716
3.00	0.745	0.0371	0.00596	0.0785

$$\phi_\beta = G_0 \int \frac{e^{-\mu'r}}{4\pi r^2} \{1 + [d_1(\mu'r) + d_2(\mu'r)^2$$

$$+ d_3(\mu'r)^3]e^{-(d_4-1)\mu'r}\} \, dV. \qquad \text{Eq. 14}$$

The integrands in Equations 7 and 14 are of the same functional form. Therefore, the evaluation of these integrals is the same for photons as it is for beta particles.

RESULTS

Photons

Values of the fitting coefficients c_1 to c_4 obtained from a least-squares fit of the expression for $B_{en}(\mu r)$ in Equation 4 to the tabulated values (13) are summarized in Table 1 for photon energies ranging from 0.015 to 3 MeV. As discussed by Berger (13), the energy grid is fine enough for interpolation to other source energies. For E $\geq$ 0.03 MeV differences between tabulated and fitted values of $B_{en}(\mu r)$ were less than 5% (range 0.05%–4.8%) for all μr. Values of $B_{en}(\mu r)$ for the two lowest photon energies, 0.015 and 0.02 MeV, in Berger's (13) tables tend to oscillate at large distances from the source ($\mu r \geq$ 13). This may due to roundoff in the calculations or to oscillations in the polynomial representation (23). At these two lowest photon energies, the maximum difference was 15% for $\mu r \geq$ 13. As discussed in (13), at large distances from the point source the dose rate is low and small oscillations in $B_{en}(\mu r)$ are without practical consequence. At smaller distances, the percent differences were in the same range as those for higher energies ($\geq$0.03 MeV). This is depicted in Figure 1 for photon energies of 0.015, 0.03 and 0.5 MeV.

Analytical calculations of absorbed fractions for spherical volume sources of photons are outlined in the Appendix by integration of Equation 7. In these calculations it is assumed that the activity is uniformly distributed within

the sphere and that the spherical source is inside an absorber of the same density and composition. The dimensions of the absorber are assumed to be large in comparison with the mean free path of photons. To test the analytical approach employed in this work, a comparison was made with the results of Monte Carlo calculations for spherical geometry. Brownell et al. (19) have employed Monte Carlo calculations to obtain absorbed fractions for central point sources in large unit-density spheres ranging in mass from 2 to 200 kg. The corresponding radii range from 7.82 to 36.3 cm.

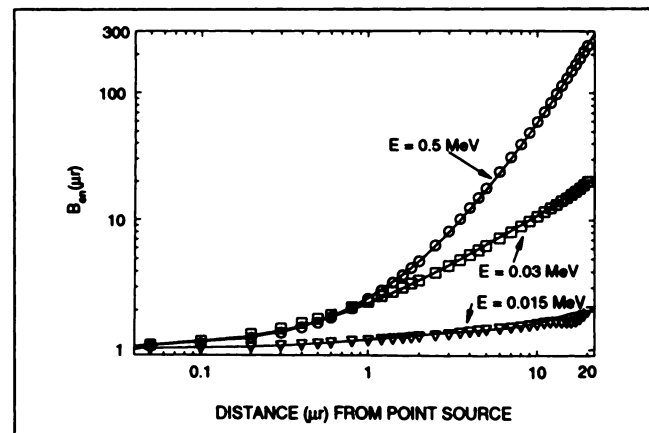Ellett and Humes (22) used a combination of Monte

FIGURE 1. Comparison of Berger's values of $B_{en}(\mu r)$ for initial photon energies of 0.015 (triangles), 0.03 (squares) and 0.5 (circles) MeV and calculations according to Equation 4. For E $\geq$ 0.03 MeV, differences between tabulated and fitted values ranged from 0.05% to 4.8%. For the two lowest initial photon energies (0.015 and 0.02 MeV), tabulated values oscillate for $\mu r \geq$ 13. For these values of μr the maximum percent difference was 15%. At smaller distances, the percent differences are in the same range as for the higher energies.
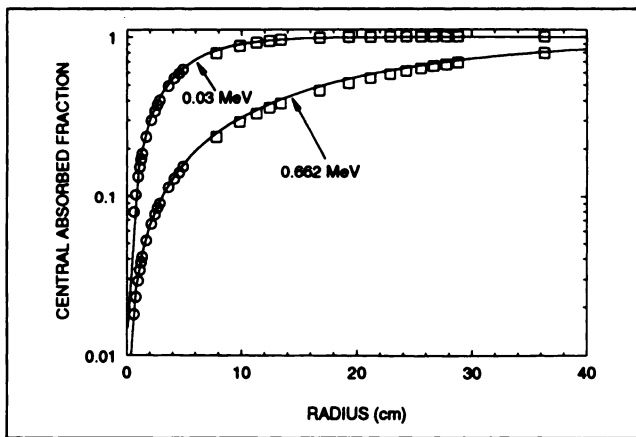
FIGURE 2. Comparison of Monte Carlo calculations of the absorbed fraction in the center of spherical source volumes and computations according to Equations A22 to A25. The initial photon energies are indicated in the figure. The radii of the spheres range from 0.62 to 36.3 cm. For unit density, the corresponding masses range from 0.001 to 200 kg. Circles are from Table 3 in (22) and squares from Table 5 in (29). Values of the coefficients required for the calculations were obtained by graphical interpolation of the data in Table 1. This yielded: $c_1 = 1.06$, $c_2 = 0.276$, $c_3 = 0.0123$, $c_4 = 0.0283$. Values of μ and μ_{en} in (22) were used in calculations.

FIGURE 3. Variation of the absorbed fraction in the center (solid lines) and on the surface (dashed lines) of spheres as a function of radius for initial photon energies of 0.015 and 0.02 MeV. The center-to-surface variation in absorbed fraction is the same as the center-to-surface absorbed-dose gradient.

Carlo and analytical techniques to determine the absorbed fraction for central point sources in small unit-density spheres with radii ranging from 0.62 to 4.92 cm. These results are summarized in Figure 2 for 0.03-MeV and 0.662-MeV photons and compared with analytical calculations based on Equations A5 and A22–A25 in the Appendix. The photon energies in Figure 2 were chosen for display because 0.03 MeV was the lowest energy considered by Ellett and Humes (22) and 0.662 MeV would appear to be an upper limit to photon energies that are of interest in nuclear medicine dosimetry. The agreement between Monte Carlo calculations and the analytical approach at other photon energies is equally good. These results validate the functional form of $B_{en}(\mu r)$ in Equation 4 and the derivations in the appendix.

The variation of the absorbed fraction for photon energies of 0.015 and 0.02 MeV as a function of radius in the range from 0.1 to 10 cm is shown in Figure 3. For both energies, the absorbed fractions in the center and on the surface were plotted because these two values represent the maximum variation in absorbed fraction for each spherical radius. For 0.015-MeV photons, the absorbed fraction in the center of the sphere is close to its maximum value of unity for spheres with a radius of ≥ 2 cm; the corresponding radius for 0.02-MeV photons is about 5 cm. If the radius is sufficiently large such that the absorbed fraction in the center is close to unity, then the absorbed fraction on the surface is approximately 65% of that in the center. For small spheres, the absorbed fraction on the surface is about 50% of that in the center. Absorbed fractions for 0.03- and 0.5-MeV photons and radii ranging from 0.1 to 40 cm are presented in Figure 4. At these higher energies, the ab-
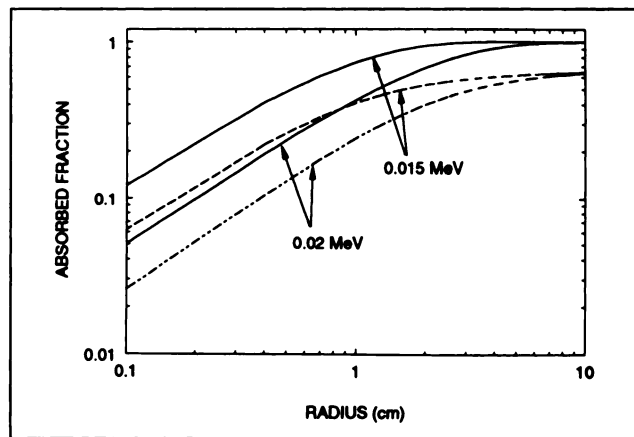
sorbed fraction in the center approaches unity at radii of about 10 cm and 40 cm for 0.03- and 0.5-MeV photons, respectively. The range of photon energies in Figures 3 and 4 includes many that are of interest in nuclear medicine dosimetry. Additional curves can be generated from the data in Table 1 and by interpolation.

Figure 5 shows the variation of the absorbed fraction as a function of distance from the center of a spherical source with a radius of 5 cm and photon energies ranging from 0.015 to 0.3 MeV. For this source radius and photon energies, the variation is small in the interior. However, the absorbed fraction decreases exponentially near the boundary and outside the spherical source volume. Absorbed-dose rates for the same photon energies and radius are depicted in Figure 6. In this figure, the activity concentration was taken to be the same for each photon energy so that the relative magnitudes of the absorbed-dose rates
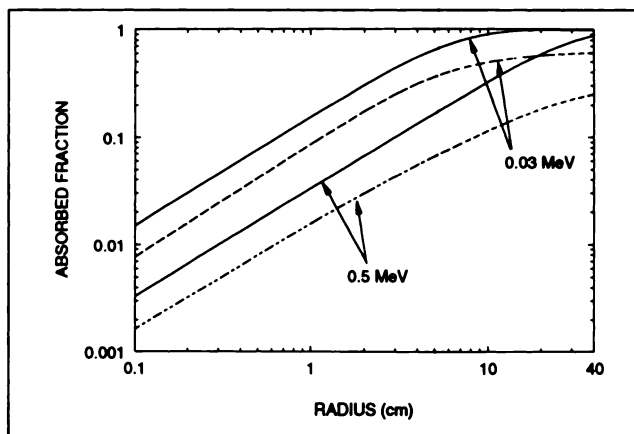

FIGURE 4. Variation of the absorbed fraction in the center (solid lines) and on the surface (dashed lines) of spheres with radii ranging from 0.1 to 40 cm. The initial photon energies are 0.03 and 0.5 MeV. For 0.5 MeV photons, the absorbed fraction in the center approaches unity for a radius of about 40 cm.
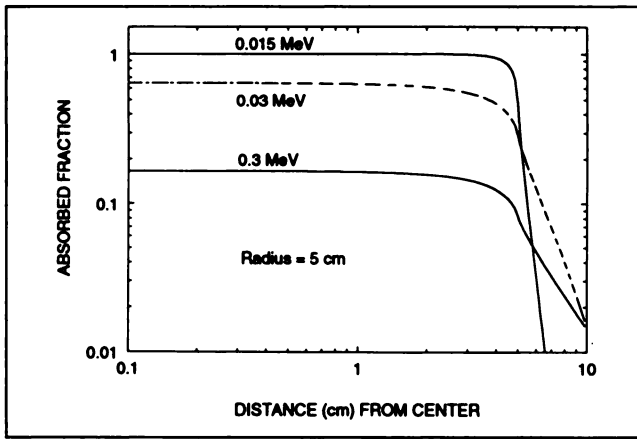
FIGURE 5. The absorbed fraction as a function of distance from the center of a sphere with a radius of 5 cm. The absorbed fractions are nearly constant in the interior of the sphere but decrease exponentially near the surface and on the outside of the sphere. The initial photon energies are indicated in the figure.

depend only on photon energy and the variation of the absorbed fraction as a function of distance from the center of the sphere.

Beta Particles

According to Equation 14, calculations of the absorbed fraction for beta particles require a knowledge of the absorption coefficient μ'. A compilation of attenuation coefficients for 14 beta particle point sources in a tissue-equivalent medium (24) was used to determine the energy dependence of μ'. The energies of the point sources ranged from 0.0057 MeV (^{3}H) to 1.43 MeV (^{106}Rh). These data and a nonlinear least-squares fit are displayed in Figure 7. The energy dependence of the absorption coefficient was determined to be
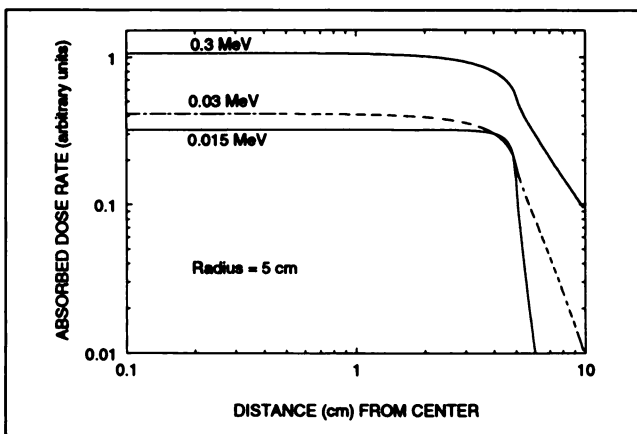

FIGURE 6. Absorbed-dose rates as a function of distance from the center of the same sphere and initial photon energies as in Figure 5. The concentration of activity within the sphere is the same for each photon energy. Under these conditions, the relative magnitude of absorbed-dose rate depends only on energy. Consequently, 0.3-MeV photons will provide the higher dose rate in spite of having the smallest absorbed fraction (Fig. 5).
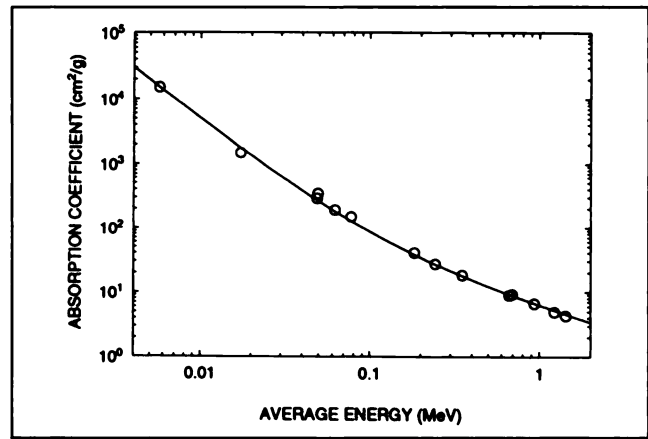

FIGURE 7. Energy dependence of the absorption coefficient μ'. Circles represent the data in (24). The line represents calculations based on Equation 15.

$$\mu' = 0.474 \ E_{av}^{-2.0} + 5.80 \ E_{av}^{-0.82}. \qquad \text{Eq. 15}$$

This formula is simpler than one previously used (3) and, as shown in Figure 7, provides a good fit over the entire energy range.

The fitting coefficients d_1 to d_4 for eight selected radionuclides, obtained from a nonlinear least-squares fit of Equation 11 to tabulated point-source data (14), are summarized in Table 2. These radionuclides were chosen because they are of interest in radionuclide therapy (6,7,10,16,17) and radiobiology (25,26) and because they span a wide range of energies. For completeness, values of the corresponding absorption coefficients are included in this table. It was shown by Leichner et al. (11) that the fitting coefficients in Table 2 yield excellent agreement with tabulated point source data (14) over the entire energy range and for a wide range of distances from point sources. Additionally, it was shown (11) that absorbed dose-rate calculations based on the function G(r) were in agreement with available results (9) for beta particles. Fitting coefficients in Equation 11 for additional radionuclides can be computed from tabulated point-source kernels (12,14).

As the integrands in Equation 7 and 14 are of the same functional form, the formulas derived for photons in the Appendix can be applied to beta particles by making the simple substitutions given.

It has been demonstrated in some experimental (27) and human studies (28) that the administration of ^{90}Y-labeled antibodies leads to improved tumor responses as compared to the treatment of the same tumors with the same antibodies but labeled with ^{131}I. This may be due to greater initial absorbed-dose rates and more uniform absorbed-dose distributions achieved with ^{90}Y than ^{131}I beta particles. However, for sufficiently small tumors, the absorbed fraction of ^{90}Y beta particles will be smaller than that of ^{131}I beta particles because of the lower energy of the latter. The methodology presented in this work permits analytical calculations of the tumor volume for which absorbed-dose rates from high-energy beta particles become equal to

TABLE 2

Numerical Values of the Fitting Coefficients d_1, d_2, d_3, d_4 and Absorption Coefficients for Selected Beta Particle Emitters

Radionuclide	d_1	d_2	d_3	d_4	μ' (cm^2/g)
^{3}H	0.581	−0.258	0.240	1.36	15,000
^{14}C	−0.585	0.722	0.0	1.36	340
^{35}S	−1.03	0.734	0.0	1.43	300
^{131}I	−1.12	1.09	0.0	1.44	40
^{111}Ag	−0.564	1.38	0.0	1.45	18
^{32}P	1.00	0.350	1.49	1.66	9.2
^{90}Y	0.684	0.114	1.38	1.59	6.6
^{106}Rh	1.01	0.490	1.40	1.61	4.2

those from low-energy beta particles. At and below this volume, high-energy beta particles provide no dose-rate advantage over low-energy beta particles. This is demonstrated in Figure 8 which shows absorbed-dose rate curves for ^{90}Y and ^{131}I beta particles at the center of spheres with radii ranging from 0.01 to 1 cm. The two curves intersect at 0.08 cm. For this radius, the absorbed fraction of ^{90}Y beta particles is sufficiently smaller than that of ^{131}I beta particles for the absorbed-dose rates inside the sphere to become equal. This result is consistent with semi-quantitative conclusions based on numerical methods (17).

Noninvasively detectable tumors are, in general, considerably larger than those just discussed. For these tumors, high-energy beta particles can offer considerable dose-rate advantages over low-energy beta particles. If the beta particle energy is completely absorbed in the interior of a tumor, which is generally the case for tumors with a radius of 0.5 cm or greater, the ratio of absorbed-dose rates is equal to the ratio of beta particle energies. For example, for equal activity concentrations, the absorbed-dose rate from ^{90}Y beta particles in the interior of such a tumor would be about five times that from ^{131}I beta particles.

The formulas for absorbed fractions of spherical source

volumes may also be applied to obtain absorbed-dose estimates on the cellular and subcellular levels. For example, the cell nucleus has been modeled as a sphere with a radius of 4 to 5 μm to obtain absorbed-dose estimates for tritiated thymidine assumed to be uniformly incorporated in the nucleus (25,26). There has been considerable discussion (26) about the uniformity of the absorbed-dose distribution in this model. The results in Figure 9 demonstrate that the absorbed fraction of tritium (^{3}H) is maximum (unity) throughout most of the nucleus and decreases to 0.5 on the surface. Consequently, the absorbed dose in this model will be uniform throughout most of the nucleus.

DISCUSSION

The results presented in this article have shown that tabulated absorbed-dose distributions around point sources of photons (13) and beta particles (14) in water can be represented analytically by relatively simple functions. Moreover, the point-source functions for photons and beta particles have the same radial dependence on distance from a point source. Consequently, calculations of absorbed-dose rate and dose can be made in a unified manner for photons and beta particles. The formulas for absorbed
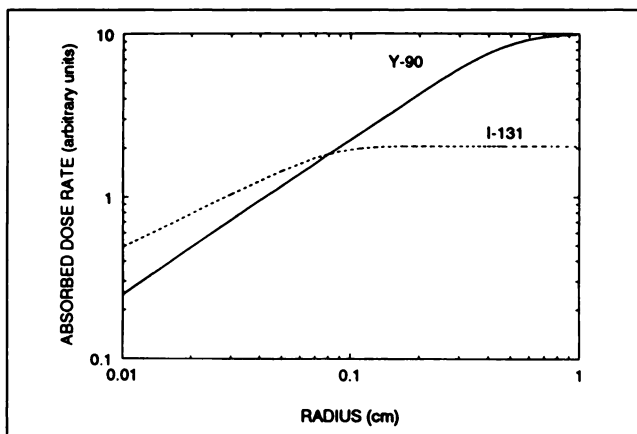

FIGURE 8. Absorbed-dose rates for ^{131}I and ^{90}Y beta particles in the center of spheres with radii ranging from 0.01 to 1 cm. The concentration of ^{131}I and ^{90}Y inside the spheres is taken to be the same. Due to the difference in beta particle energies of these radionuclides, the curves intersect at a radius of 0.08 cm.
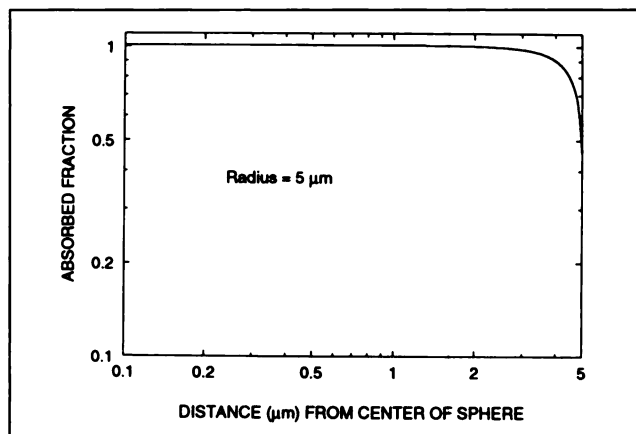

FIGURE 9. Variation in the absorbed fraction for ^{3}H inside a cell nucleus, modeled as a sphere of radius μm. The absorbed fraction is at its maximum value of 1 throughout most of the nucleus. Therefore, the absorbed-dose rate will be constant for most of this model nucleus.

fractions were evaluated explicitly for spherical geometry to determine absorbed dose rates as a function of distance from the center within and outside of spherical source volumes. As shown in the Appendix, a unified approach to photon and beta particle dosimetry provides considerable calculational advantages because only a few parameters need to be changed in applying formulas to both photons and beta particles. This should prove particularly useful for tumor dosimetry in radionuclide therapy. Additionally, the solutions presented in the Appendix can be used to calculate absorbed dose rates for any finite volume, including those that are of interest in radiobiological investigations.

Absorbed fractions for photons have usually been expressed as a simple ratio of the photon energy absorbed by the target-to-the photon energy emitted by the source. Therefore, it was possible to only compare the analytical solution for the absorbed fraction at the center of spheres with Monte Carlo calculations (19,22). The agreement between the two methods of calculation (Fig. 2) has validated the approach used in this study, consistent with the dose reciprocity theorem (3). The dose reciprocity theorem states that the absorbed dose at a point due to a uniform distribution of activity equals the mean absorbed dose in this volume due to the same activity concentrated at that point. Hence, the absorbed fraction in the center of a sphere containing a uniform distribution of activity is equal to the absorbed fraction for a central point source in that sphere.

The results have also demonstrated (Figs. 3–6) that there are absorbed-dose gradients in going from the center of a spherical source to the surface. Consequently, the absorbed fractions for photons are more than simple ratios, and the variation of the absorbed fraction as a function of distance from the center should be included in absorbed-dose calculations. Absorbed-dose gradients have not been taken into account in available tables of S factors (30). It is currently not known how much of an effect on absorbed-dose calculations such gradients would have for various source-and-target configurations.

The advantage of point-source functions and analytical solutions of dosimetry problems is that calculations can be made rapidly and without approximation. All of the numerical results presented in Figures 1–9 were obtained on a personal computer. Of course, analytical solutions are possible for only a few geometries such as spheres, cylinders, line and plane sources (1–6,8,9,11). For irregular volumes and nonuniform activity distributions, numerical methods need to be employed (7,17).

The results for beta particles presented in this article demonstrate explicitly that the MIRD schema (18) is not limited to macrodosimetry and that model calculations can be made for any finite volume, including the cell nucleus. Moreover, the analytical point-source function technique developed in this article is not limited to beta emitters in Berger's tables (14). The same method of analysis can be applied to other publications on absorbed-dose distributions for beta particles (12,31).

APPENDIX

The purpose of this appendix is to outline the derivation of formulas for absorbed fractions for spherical geometry.

Photons

According to Equation 7, for photons this requires an evaluation of the integral

$$\phi = \mu_{en} \int \frac{e^{-\mu r}}{4\pi r^2} \{1 + [c_1(\mu r) + c_2(\mu r)^2 + c_3(\mu r)^3] e^{-c_4\mu r}\} \, dV.$$

Eq. A1

The geometry is well understood (1,5,25,26) and depicted in Figure 10. The absorbed dose is to be calculated at a point P located at a distance b from the center of a sphere of radius a. Figure 10 shows geometric configurations for P outside and inside the sphere. The volume elements inside and outside the sphere are defined as follows:

Inside

$$dV = 4\pi r^2 dr \qquad 0 \le r \le a - b \qquad \text{Eq. A2}$$

$$dV = (\pi r/b)[a^2 - (b - r)^2]dr \qquad a - b < r \le a + b \qquad \text{Eq. A3}$$

and outside

$$dV = (\pi r/b)[a^2 - (b - r)^2]dr \qquad a \le b. \qquad \text{Eq. A4}$$

To make the derivation more tractable, Equation A1 is divided into four parts:

$$\phi = \mu_{en} \sum_{i=0}^{3} \phi_i \qquad \text{Eq. A5}$$

with

$$\phi_0 = \int \frac{e^{-\mu r}}{4\pi r^2} \, dV, \qquad \text{Eq. A6}$$

$$\phi_1 = \int \frac{e^{-c\mu r}}{4\pi r^2} c_1(\mu r) \, dV, \qquad \text{Eq. A7}$$

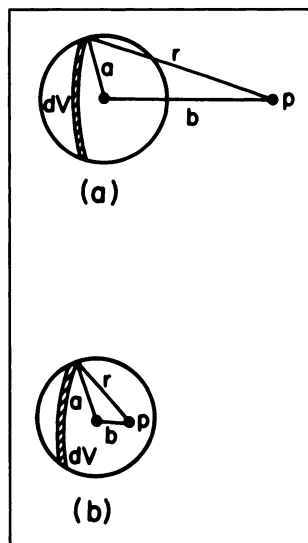$$\phi_2 = \int \frac{e^{-c\mu r}}{4\pi r^2} c_2(\mu r)^2 \, dV, \qquad \text{Eq. A8}$$

FIGURE 10. Notation used in the definition of volume elements dV and the derivation of equations in the appendix. The absorbed dose is calculated at point P which is at a distance b from the center of a sphere of radius a (a and b depict the configurations with p outside and inside the sphere, respectively).

and

$$\phi_3 = \int \frac{e^{-c\mu r}}{4\pi r^2} c_3(\mu r)^3 \, dV. \qquad \text{Eq. A9}$$

In Equations A7 to A9, $c = 1 + c_4$. For additional tractability and consistent with the volume elements defined above, it is useful to distinguish between the absorbed fraction inside and outside the sphere. From Equations A2, A3 and A6 it follows that the expression for ϕ_0 inside the sphere involves integrals of the type

$$\int_0^{a-b} \frac{e^{-\mu r}}{r} \, dr + \frac{1}{4b} \int_{a-b}^{a+b} \frac{[a^2 - (b-r)^2]}{r} e^{-\mu r} \, dr. \qquad \text{Eq. A10}$$

This requires the evaluation of an integral of the form

$$\int_{a-b}^{a+b} \frac{e^{-\mu r}}{r} \, dr = \int_{a-b}^{\infty} \frac{e^{-\mu r}}{r} \, dr - \int_{a+b}^{\infty} \frac{e^{-\mu r}}{r} \, dr. \qquad \text{Eq. A11}$$

It has been shown (1,5,11) that

$$\int_{a-b}^{\infty} e^{-\mu r} \, dr = E_1[\mu(a-b)], \qquad \text{Eq. A12}$$

where E_1 is the exponential integral (29). Hence, Equation A11 becomes

$$\int_{a-b}^{a+b} \frac{e^{-\mu r}}{r} \, dr = E_1[\mu(a-b)] - E_1[\mu(a+b)]. \qquad \text{Eq. A13}$$

In numerical computations, Formulas 5.1.53 and 5.1.54 in (29) are useful. The remaining integrals in Equations A6–A9 are integrable in closed form using standard formulas. After rearranging and simplifying terms, the following expression is obtained for ϕ_0 inside the sphere, $\phi_0(\text{ins})$:

$$\phi_0(\text{ins}) = \frac{1}{4\mu^2 b}\{4\mu b + [1 + \mu(a-b)]e^{-\mu(a+b)} - [1 + \mu(a+b)]$$

$$\cdot e^{-\mu(a-b)}\} + \frac{a^2 - b^2}{4b}\{E_1[\mu(a-b)] - E_1[\mu(a+b)]\} \quad \text{Eq. A14}$$

This result is consistent with previous work (1,5). The remaining terms for the absorbed fraction inside the sphere are:

$$\phi_1(\text{ins}) = \frac{c_1}{2bc^3\mu^2}\{2c\mu b + (1 + c\mu a)[e^{-c\mu(a+b)} - e^{-c\mu(a-b)}]\},$$

$$\text{Eq. A15}$$

$$\phi_2(\text{ins}) = \frac{c_2}{2bc^4\mu^2}\{4c\mu b + [c^2\mu^2 a(a+b) + c\mu(3a+b) + 3]$$

$$\cdot e^{-c\mu(a+b)} - [c^2\mu^2 a(a-b) + c\mu(3a-b) + 3]e^{-c\mu(a-b)}\},$$

$$\text{Eq. A16}$$

$$\phi_3(\text{ins}) = \frac{c_3}{2bc^5\mu^2}\{12c\mu b + [c^3\mu^3 a(a+b)^2 + c^2\mu^2(5a^2 + b^2$$

$$+ 6ab) + 6c\mu(2a+b) + 12]e^{-c\mu(a+b)} - [c^3\mu^3 a(a-b)^2$$

$$+ c^2\mu^2(5a^2 + b^2 - 6ab) + 6c\mu(2a-b) + 12]e^{-c\mu(a-b)}\}.$$

$$\text{Eq. A17}$$

The photon absorbed fraction inside the sphere as a function of the distance b from the center is obtained by summing over the last four equations and multiplying by μ_{en} as indicated in Equation A5.

Evaluation of the integrals for the absorbed fraction outside the sphere proceeds in the same manner as inside, with limits of integration ranging from $b - a$ to $b + a$ (26). The results are:

$$\phi_0(\text{out}) = \frac{1}{4\mu^2 b}\{[1 - \mu(b-a)]e^{-\mu(b+a)}$$

$$- [1 - \mu(b+a)]e^{-\mu(b-a)}\} + \frac{a^2 - b^2}{4b}$$

$$\cdot \{E_1[\mu(b-a)] - E_1[\mu(b+a)]\}, \qquad \text{Eq. A18}$$

$$\phi_1(\text{out}) = \frac{c_1}{2bc^3\mu^2}[(1 + c\mu a)e^{-c\mu(b+a)} - (1 - c\mu a)e^{-c\mu(b-a)}],$$

$$\text{Eq. A19}$$

$$\phi_2(\text{out}) = \frac{c_2}{2bc^4\mu^2}\{[c^2\mu^2 a(a+b) + c\mu(3a+b) + 3]e^{-c\mu(a+b)}$$

$$- [c^2\mu^2 a(a-b) + c\mu(b-3a) + 3]e^{-c\mu(b-a)}\}, \quad \text{Eq. A20}$$

$$\phi_3(\text{out}) = \frac{c_3}{2bc^5\mu^2}\{[c^3\mu^3 a(a+b)^2 + c^2\mu^2(5a^2 + b^2 + 6ab)$$

$$+ 6c\mu(2a+b) + 12]e^{-c\mu(a-b)} - [-c^3\mu^3 a(b-a)^2$$

$$+ c^2\mu^2(5a^2 + b^2 - 6ab) + 6c\mu(b-2a) + 12]e^{-c\mu(b-a)}\}.$$

$$\text{Eq. A21}$$

The photon absorbed fraction outside the sphere is obtained by carrying out the summation indicated in Equation A5.

In special cases, the formulas for absorbed fractions simplify considerably. The absorbed fraction at the center of a sphere is obtained from Equations A14–A17 by taking the limit as b approaches zero. This leads to the following relations:

$$\phi_0(\text{cent}) = \frac{1}{\mu}(1 - e^{-\mu a}), \qquad \text{Eq. A22}$$

$$\phi_1(\text{cent}) = \frac{c_1}{c^2\mu}[1 - (1 + c\mu a)e^{-c\mu a}], \qquad \text{Eq. A23}$$

$$\phi_2(\text{cent}) = \frac{c_2}{c^3\mu}\{2 - [(c\mu a)^2 + 2(c\mu a + 1)]e^{-c\mu a}\}, \qquad \text{Eq. A24}$$

$$\phi_3(\text{cent}) = \frac{c_3}{c^4\mu}\{6 - [6 + c\mu a(c^2\mu^2 a^2 + 3c\mu a + 6)]e^{-c\mu a}\}. \qquad \text{Eq. A25}$$

As the radius a goes to zero, the last four equations correctly go to zero. The photon absorbed fraction in the center is obtained by substituting the last four equations in Equation A5.

The absorbed fraction on the surface of a sphere is obtained from Equations A14–A17 or A18–A21 by setting $a = b$. This yields

$$\phi_0(\text{surf}) = \frac{1}{4\mu^2 a}(e^{-2\mu a} + 2\mu a - 1), \qquad \text{Eq. A26}$$

$$\phi_1(\text{surf}) = \frac{c_1}{2c^3\mu^2 a} [(1 + c\mu a)e^{-2c\mu a} + c\mu a - 1], \qquad \text{Eq. A27}$$

$$\phi_2(\text{surf}) = \frac{c_2}{2c^4\mu^2 a} [2c\mu a - 3 + (2c^2\mu^2 a^2 + 4c\mu a + 3)e^{-2c\mu a}], \qquad \text{Eq. A28}$$

$$\phi_3(\text{surf}) = \frac{3c_3}{c^5\mu^2 a} \left\{ c\mu a - 2 + \left[\frac{2}{3} (c\mu a)^3 + 2(c\mu a)^2 + 3c\mu a + 2\right]e^{-2c\mu a} \right\}. \qquad \text{Eq. A29}$$

Beta Particles

From Equations 14 and A5 it follows that the absorbed fractions for beta particles may be written as

$$\phi_\beta = G_0 \sum_{k=0}^{3} \phi_\beta^{(k)} \qquad \text{Eq. A30}$$

with

$$\phi_\beta^{(0)} = \int \frac{e^{-\mu' r}}{4\pi r^2} dV, \qquad \text{Eq. A31}$$

$$\phi_\beta^{(1)} = \int \frac{e^{-d_4\mu' r}}{4\pi r^2} d_1(\mu' r) dV, \qquad \text{Eq. A32}$$

$$\phi_\beta^{(2)} = \int \frac{e^{-d_4\mu' r}}{4\pi r^2} d_2(\mu' r)^2 dV, \qquad \text{Eq. A33}$$

$$\phi_\beta^{(3)} = \int \frac{e^{-d_4\mu' r}}{4\pi r^2} d_3(\mu' r)^3 dV. \qquad \text{Eq. A34}$$

From Equations A6–A9 and A31–A34 it follows that the expressions given above for the photon absorbed fractions within, outside, in the center, and on the surface of a sphere may be applied directly to beta particles *provided* that the following substitutions are made: $\mu \to \mu'$ (μ is replaced by μ'), $\mu_{en} \to G_0$, $c_1 \to d_1$, $c_2 \to d_2$, $c_3 \to d_3$ and $c \to d_4$.

ACKNOWLEDGMENT

REFERENCES

1. Rossi HH, Ellis RH Jr. Distributed beta sources in uniformly absorbing media: I. *Nucleonics* 1950;7:18–25.
2. Rossi HH, Ellis RH Jr. Distributed beta sources in uniformly absorbing media: II. *Nucleonics* 1950;7:19–25.
3. Loevinger R, Japha EM, Brownell GL. Discrete radioisotope sources. In: Hine GJ, Brownell GL, eds. *Radiation dosimetry*. New York: Academic Press; 1956:693–799.
4. Berger MJ. Beta-ray dosimetry calculations with the use of point kernels. In: Cloutier RJ, Edwards CL, Snyder WS, eds. *Medical radionuclides: radiation dose and effects*. Oak Ridge, TN: AEC symposium series No. 20, CONF 691212; 1970:63–86.
5. Oddie TH. Dosages from radioisotopes uniformly distributed within a sphere. *Br J Radiology* 1951;24:333–336.

6. Leichner PK, Cash SA, Backx D, Durand RE. Effects of injection volume on tissue dose, dose rate, and therapeutic potential of intraperitoneal ^{32}P. *Radiology* 1981;141:193–199.
7. Kwok CS, Prestwich WV, Wilson BC. Calculation of radiation doses for nonuniformaly distributed β and γ radionuclides in soft tissue. *Med Phys* 1985;12:405–412.
8. Vynkier S, Wambersie A. Dosimetry of beta sources in radiotherapy: absorbed dose distributions around plane sources. *Rad Prot Dosim* 1985;13:249–252.
9. Cross WG, Ing H, Freedman NO, Mainville J. Tables of beta-ray distributions in water, air, and other media. Chalk River Nuclear Laboratories, Chalk River, Ontario, Canada: Atomic Energy of Canada, Ltd, Report No. AECL-7617: 1982:1–89.
10. Kwok CS, Irfan M, Chan LB, Prestwich WV. Beta dosimetry for radioimmunotherapy of cancer using radiolabeled antibodies. *NCI Monographs* 1987;3:73–82.
11. Leichner PK, Hawkins WG, Yang N-C. A generalized empirical point-source function for beta particle dosimetry. *Antibody Immunoconj Radiopharm* 1989;2:125–144.
12. Prestwich WV, Nunes J, Kwok CS. Beta dose point kernels for radionuclides of potential use in radioimmunotherapy. *J Nucl Med* 1989;30:1036–1046.
13. Berger MJ. Energy deposition in water by photons from point isotropic sources. *MIRD pamphlet no. 2*. New York: Society of Nuclear Medicine, 1968:17–25.
14. Berger MJ. Distribution of absorbed dose around point sources of electrons and beta particles in water and other media. *MIRD pamphlet no. 7*. New York: Society of Nuclear Medicine, 1971:7–32.
15. Johnson TK. MABDOS: a generalized program for internal radionuclide dosimetry. *Comput Math Prog Biomed* 1988;27:159–167.
16. Siegel JA, Pawlyk DA, Lee RE, et al. Tumor, red marrow, and organ dosimetry for ^{131}I-labeled anti-carcinoembryonic antigen monoclonal antibody. *Cancer Res* 1990;50(suppl):1039s–1042s.
17. Langmuir VK, Sutherland RM. Dosimetry models for radioimmunotherapy. *Med Phys* 1988;15:867–873.
18. Loevinger R, Berman M. A revised schema for calculating the absorbed dose from biologically distributed radionuclides. *MIRD pamphlet no. 1*, revised. New York: Society of Nuclear Medicine; 1976:3–10.
19. Brownell GL, Ellett WH, Reddy AR. Absorbed fractions for photon dosimetry. *MIRD pamphlet no. 3*. New York: Society of Nuclear Medicine; 1968:28–39.
20. Marquardt DW. An algorithm for least-squares estimation of nonlinear parameters. *J Soc Ind Appl Math* 1963;11:431–441.
21. Press WH, Flannery BP, Teukolsky SA, Vetterling WT. *Numerical recipes—the art of scientific computing*. New York: Cambridge University Press; 1986:523–527.
22. Ellett WH, Humes RM. Absorbed fractions for small volumes containing photon-emitting radioactivity. *MIRD pamphlet no. 8*. New York: Society of Nuclear Medicine; 1971:27–32.
23. Valley JF, Kushelevsky, Lerch P. A method for the calculation of beta-ray dose. *Health Phys* 1974;26:295–300.
24. Bochkarev VV, Radzievsky GB, Timofeev LV, Demianov NA. Distribution of absorbed energy from a point beta source in a tissue-equivalent medium. *Int J Appl Radiat Isotopes* 1972;23:493–504.
25. Tägder K, Scheuermann W. Estimation of absorbed doses in the cell nucleus after incorporation of ^{3}H- or ^{14}C-labeled thymidine. *Radiat Res* 1970; 41:202–216.
26. Bleecken S. Tritium-mikrodosimetry. *Strahlentherapy* 1964;125:145–157.
27. Klein JL, Nguyen TH, Laroque P, et al. Yttrium-90 and iodine-131 radioimmunoglobulin therapy of an experimental hepatoma. *Cancer Res* 1989; 43:6383–6389.
28. Vriesendorp HM, Herpst JM, Germack MA, et al. Phase I-II studies of yttrium-labeled antiferritin treatment for endstage Hodgkin's disease including RTOG 87-01. *J Clin Oncol* 1991;9:918–928.
29. Gautsch W, Cahill WF. Exponential integral and related functions. In: Abramowitz M, Stegum IA, eds. *Handbook of mathematical functions*. New York: Dover Publications; 1972:227–237.
30. Snyder WS, Ford MR, Warner GG, Watson SB. "S," absorbed dose per unit per unit cumulated activity for selected radionuclides and organs. *MIRD pamphlet no. 11*. New York: Society of Nuclear Medicine; 1975:5–257.
31. Simpkin DJ, Mackie TR. EGS4 Monte Carlo determinations of the beta dose point kernel in water. *Med Phys* 1990;17:179–186.